ACS OMEGA

http://pubs.acs.org/journal/acsodf

Article

Sodium/Lithium-Ion Transfer Reaction at the Interface between Low-Crystallized Carbon Nanosphere Electrodes and Organic Electrolytes

Yasuyuki Kondo,* Tomokazu Fukutsuka, Yuko Yokoyama, Yuto Miyahara, Kohei Miyazaki, and Takeshi Abe

Cite This: *ACS Omega* 2021, 6, 18737−18744

Read Online

ACCESS | Metrics & More | Article Recommendations

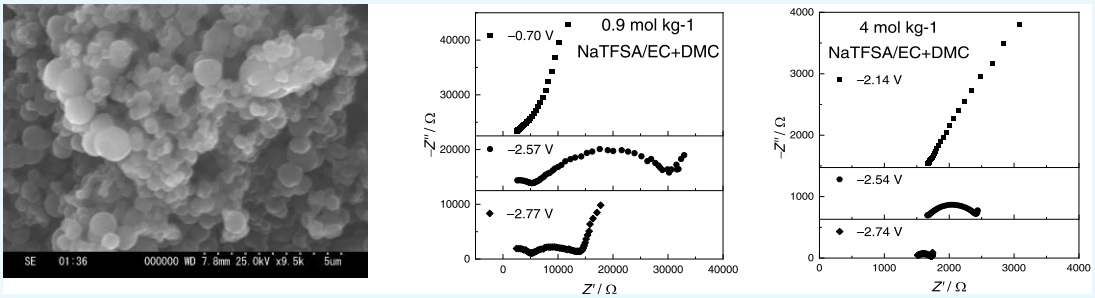

ABSTRACT: Carbon nanosphere (CNS) electrodes are the candidate of sodium-ion battery (SIB) negative electrodes with small internal resistances due to their small particle sizes. Electrochemical properties of low-crystallized CNS electrodes in dilute and concentrated sodium bis(trifluoromethanesulfonyl) amide/ethylene carbonate + dimethyl carbonate (NaTFSA/EC + DMC) were first investigated. From the cyclic voltammograms, both lithium ion and sodium ion can reversibly insert into/from CNSs in all of the electrolytes used here. The cycling stability of CNSs in concentrated electrolytes was better than that in dilute electrolytes for the SIB system. The interfacial charge-transfer resistances at the interface between CNSs and organic electrolytes were evaluated using electrochemical impedance spectroscopy. In the Nyquist plots, the semicircles at the middle-frequency region were assigned to the parallel circuits of charge-transfer resistances and capacitances. The interfacial sodium-ion transfer resistances in concentrated organic electrolytes were much smaller than those in dilute electrolytes, and the rate capability of CNS electrodes in sodium salt-concentrated electrolytes might be better than in dilute electrolytes, suggesting that CNSs with concentrated electrolytes are the candidate of SIB negative electrode materials with high rate capability. The calculated activation energies of interfacial sodium-ion transfer were dependent on electrolyte compositions and similar to those of interfacial lithium-ion transfer.

1. INTRODUCTION

Global energy consumption has continued to increase with the economic growth of emerging countries, and the emission of greenhouse gases has increased. To suppress greenhouse gas emissions without impeding the economic growth of emerging countries, it is essential to shift from the thermal power generation to the renewable energy generation.[1] Because the power generation by renewable energies usually fluctuates drastically, the large-scale power energy storage is necessary. In addition, electric vehicles (EVs) are also paid much attention owing to decreased emission of carbon dioxide. Currently, the lithium-ion batteries (LIBs) are used for the electric motors of EVs,[2] and the next-generation LIBs with high energy densities are developed.[3,4] At the same time, the increase of cost and the shortage of lithium sources are predicted after LIBs are widely applied to these large-scale applications. Then, sodium-ion batteries (SIBs) are attracting attention as substitutes for LIBs because of abundant sodium resources.[5] The configuration of SIBs is originated from the concept that the lithium ion in the LIBs is replaced with the sodium ion. Sodium ion shuttles between positive electrodes and negative electrodes in SIBs in the same manner as in LIBs. The candidates of negative electrode materials of SIBs are carbonaceous materials, titanium-based materials, phosphorus, or tin.[6] Among these materials, carbonaceous materials are the most attractive as they are commercialized for LIBs. The most famous candidate for carbon negative electrode material in SIBs is amorphous carbon because

Received: April 1, 2021
Accepted: July 5, 2021
Published: July 13, 2021

the reactivity of sodium ion and graphitic materials is anomalously small and sodium ion cannot insert into graphite but inserts deeply into amorphous carbon.[7]

As for the batteries of EVs, high rate capability is also desired. Carbon nanosphere (CNS) is expected as the candidate for carbon negative electrode materials with high rate capability and good cycling stability because CNS has small particle sizes, short diffusion distances, and the basal planes covering the surface.[8,9] To enhance the rate capability of electrode materials, the resistance of electron transfer in composite electrodes, the resistance of ion diffusion in composite electrodes, the resistance of ion diffusion inside the electrode material, and the resistance of interfacial ion transfer should be considered.[10] To analyze each resistance inside batteries, electrochemical alternating current impedance spectroscopy is the specific tool because processes with different relaxation times can be divided by impedance spectroscopy.[11] In LIBs, the interfacial lithium-ion transfer reaction at the interface between electrodes and electrolytes has been studied using electrochemical impedance spectroscopy.[12−15] Based on these results, the interfacial lithium-ion transfer is especially the significant rate-determining step. The interfacial sodium-ion transfer at the interface between electrodes and electrolytes is also expected to be the significant step. However, the kinetic properties of interfacial sodium-ion transfer at the interface between the CNS electrode and electrolyte are still not fully understood.

The kinetics of lithium-ion transfer at the interface between graphite negative electrodes and electrolyte solutions seemed to be influenced by the interaction between lithium ions and solvents, counteranions, or solid electrolyte interphase (SEI) in common organic electrolyte solutions, organic electrolyte solutions with SEI-forming additives like vinylene carbonate or fluoroethylene carbonate (FEC), and ionic liquid-based electrolyte solutions, respectively.[12−14] As for ordinal ethylene carbonate (EC)-based electrolyte solutions, the rate-determining process in the interfacial lithium-ion transfer seemed to be the desolvation process of lithium ions.[15] On the other hand, the kinetics of sodium-ion transfer at the interface between CNS electrodes and electrolyte solutions is complicated. In the previous study, the interaction between sodium ions and organic solvents was expected to be weaker than the interaction between lithium ions and solvents.[16] On the contrary, the activation energies of the interfacial sodium-ion transfer at the interface between graphitized CNS electrodes and electrolyte solutions were as large as those of interfacial lithium-ion transfer.[17] In addition, the activation energies were dependent on the composition of electrolyte solutions.[17] However, the interfacial sodium-ion transfer resistances of CNS electrodes measured in the previous study were much larger than the interfacial lithium-ion transfer resistances even if amorphous CNS electrodes, which seemed to have many reactive sites, were used with FEC-based electrolytes. Therefore, discovering the proper electrolytes to decrease the sodium-ion transfer resistances of amorphous CNS electrodes is still necessary.

In this study, the interfacial sodium-ion transfer resistances and the activation energies of sodium-ion transfer reaction at the interface between amorphous CNS electrodes and EC-based organic electrolyte solutions were measured by electrochemical impedance spectroscopy. The EC-based electrolyte with ordinal concentration was first used because it is the most common organic electrolyte. The EC-based electrolyte with high salt concentration was also used to make SEI more stable and prevent degradation, as reported in previous studies.[4,18] As a comparison, the interfacial lithium-ion transfer reaction at the interface between amorphous CNS electrodes and organic electrolyte solutions was also investigated.

2. RESULTS AND DISCUSSION

2.1. Structural Characterization of CNS-1100. First, the structure of CNS-1100 (CNS treated at 1100 °C) was investigated. Figure 1 shows the X-ray diffraction (XRD) pattern of CNS-1100. The XRD pattern of CNS-1100 did not show the (002) line derived from the graphitic structure.[19] Figure 2 shows the Raman spectrum of CNS-1100 electrodes.

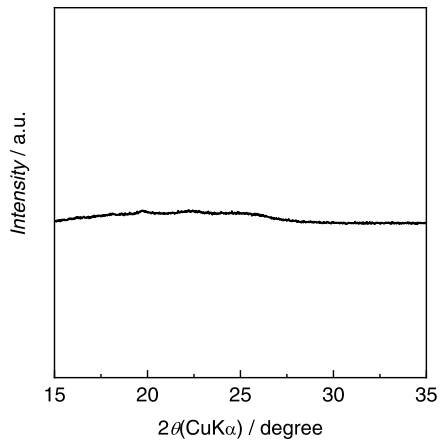

Figure 1. XRD pattern of the CNS-1100 electrode.

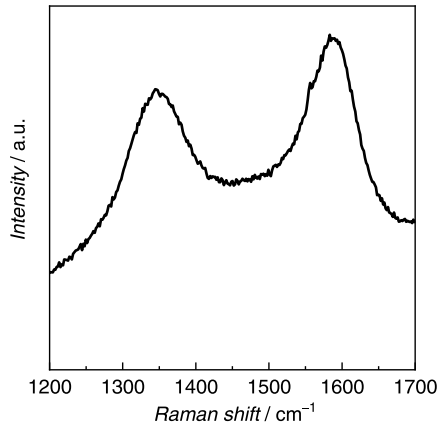

Figure 2. Raman spectrum of the CNS-1100 electrode.

The Raman spectrum showed a large D-band[9] at around 1350 cm^{-1} and a G-band[9] at around 1585 cm^{-1}. These results indicated that CNS-1100 had an amorphous and low graphitized structure in both bulk and surface regions, as previously reported.[9,19] Figure 3 shows the scanning electron microscopy (SEM) image of CNS-1100 composite electrodes. CNS-1100 had a spherical shape indicating the coverage by bent basal planes derived from low graphitization degree, and the lithium ion or sodium ion intercalates into CNS-1100 from the surface of CNS. The solution structures of organic electrolytes were also investigated using Raman spectroscopy. Figure 4 shows the Raman spectra of 0.9 and 4 mol kg^{-1} lithium bis(trifluoromethanesulfonyl) amide/ethylene carbonate + dimethyl carbonate (LiTFSA/EC + DMC) and 0.9 and 4 mol kg^{-1} sodium bis(trifluoromethanesulfonyl) amide/EC + DMC

https://doi.org/10.1021/acsomega.1c01751
ACS Omega 2021, 6, 18737−18744

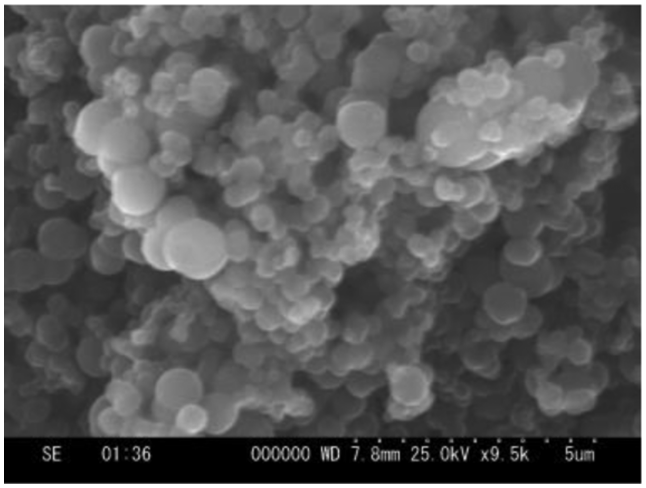

Figure 3. SEM image of the CNS-1100 electrode.

(NaTFSA/EC + DMC). The peaks derived from C═O bending modes[20] of EC and CF_3 bending modes[21] of the TFSA anion appeared at around 720 and 745 cm^{-1}, respectively. These peaks shifted at a higher Raman shift in concentrated electrolytes by the interaction with lithium or sodium ion, indicating that most of the lithium or sodium ions were coordinated with solvents in dilute electrolytes or anions in concentrated electrolytes.

2.2. Lithium-Ion Transfer Reaction at the Interface between CNS Composite Electrodes/Organic Electrolyte Solutions. Electrochemical properties of CNS-1100 composite electrodes in electrolytes containing lithium ions were investigated. Figure 5 shows the CVs of 0.9 and 4 mol kg^{-1} CNS-1100 composite electrodes in LiTFSA/EC + DMC. The irreversible currents were observed only in the 1st cycle, suggesting the formation of SEI on CNS electrodes in all of the electrolytes. The redox peaks also appeared in all of the electrolytes and were assigned to the reversible lithium-ion insertion into/from CNS-1100.

Figure 6 shows the Nyquist plots of the CNS-1100 composite electrode in 0.9 and 4 mol kg^{-1} LiTFSA/EC + DMC (1:1 by vol). Two semicircles appeared at the high-frequency and the middle-frequency regions in 0.9 mol kg^{-1} LiTFSA/EC + DMC (1:1 by vol). The semicircles at the high-frequency region or at the middle-frequency region were assigned to the parallel circuits of capacitances and SEI resistances or charge-transfer resistances, respectively, because only the semicircle at the high frequency was observed at open-circuit potential (OCV) after cyclic voltammetry (CV). Only one semicircle was observed at the middle-frequency region in 4 mol kg^{-1} LiTFSA/EC + DMC (1:1 by vol). As for the concentrated electrolytes, this semicircle was assigned to the charge-transfer resistance. The SEI resistance seemed to be negligibly small in the concentrated electrolyte because the SEI on CNS electrodes in this concentrated electrolyte might have good passivation ability than in 0.9 mol kg^{-1} LiTFSA/EC + DMC (1:1 by vol), and the SEI formation reaction might finish earlier and the thickness of SEI in the concentrated electrolyte might be thinner than in the dilute electrolyte, as previously reported for concentrated carbonate-based electrolytes.[22]

The activation energies of the interfacial lithium-ion transfer at the interface between CNS and electrolyte solutions were measured. The logarithmic reciprocal of charge-transfer resistances was plotted against the reciprocal of temperature. Figure 7 shows the temperature dependence of charge-transfer reactions of CNS-1100 composite electrodes in 0.9 and 4 mol kg^{-1} LiTFSA/EC + DMC (1:1 by vol). The activation energy was calculated using the following Arrhenius equation[13]

$$\frac{T}{R_{ct}} = A \exp\left(-\frac{E_a}{RT}\right) \quad (1)$$

where R_{ct} is the charge-transfer resistance, A is the prefrequency factor, E_a is the activation energy, R is the gas constant, and T is

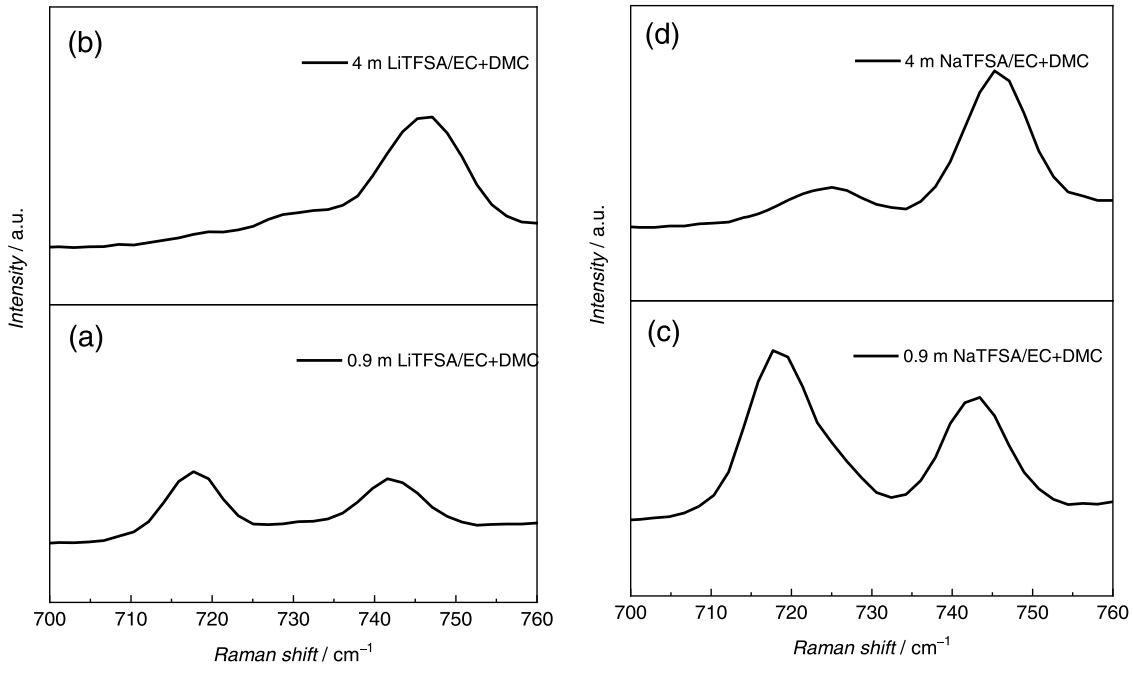

Figure 4. Raman spectra of (a) 0.9 and (b) 4 mol kg^{-1} LiTFSA/EC + DMC and (c) 0.9 and (d) 4 mol kg^{-1} NaTFSA/EC + DMC.

https://doi.org/10.1021/acsomega.1c01751
ACS Omega 2021, 6, 18737−18744

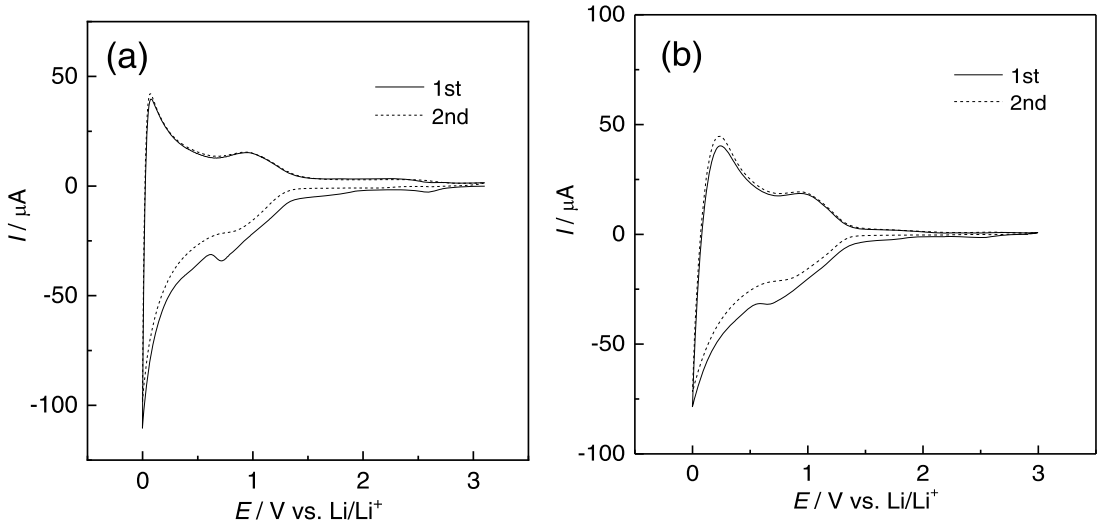

Figure 5. Cyclic voltammograms of the CNS-1100 composite electrode in (a) 0.9 and (b) 4 mol kg^{-1} LiTFSA/EC + DMC (1:1 by vol) at a scan rate of 0.1 mV s^{-1}.

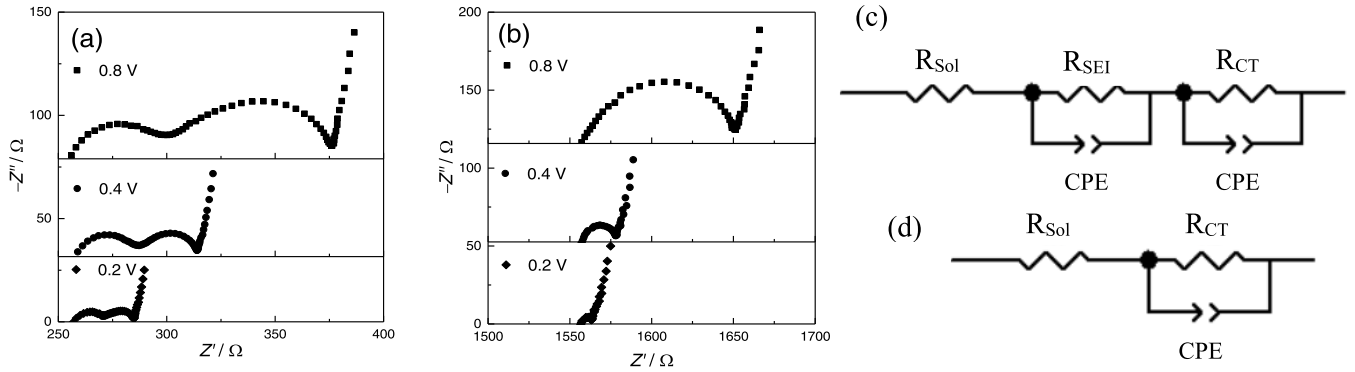

Figure 6. Nyquist plots of CNS-1100 composite electrodes in (a) 0.9 and (b) 4 mol kg^{-1} LiTFSA/EC + DMC (1:1 by vol) and equivalent circuits used for fitting for CNS-1100 electrodes in (c) 0.9 and (d) 4 mol kg^{-1} LiTFSA/EC + DMC (1:1 by vol).

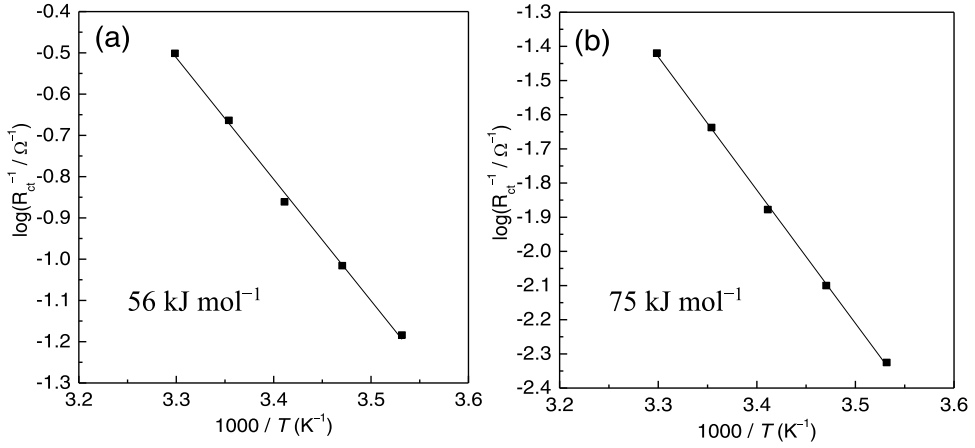

Figure 7. Temperature dependence of charge-transfer resistances of CNS-1100 composite electrodes in (a) 0.9 and (b) 4 mol kg^{-1} LiTFSA/EC + DMC (1:1 by vol).

the absolute temperature. The charge-transfer resistances were estimated basically by fitting with the equivalent circuit shown in Figure 6c (R_{Sol} is the resistance of electrolyte conductivity and R_{SEI} is SEI resistance). When the SEI resistance was negligible, the charge-transfer resistances were estimated using the equivalent circuit shown in Figure 6d. As a result, the activation energy in 0.9 mol kg^{-1} LiTFSA/EC + DMC (1:1 by vol) was 56 kJ mol^{-1}, which was near to the reported values for highly oriented pyrolytic graphite (HOPG) and glassy carbon electrodes.[23,24] In the previous reports regarding the lithium-ion transfer resistances of carbon negative electrodes, the differences in activation energies of charge-transfer resistances measured in different electrolytes corresponded to the differences of interaction between lithium ions and solvents by

https://doi.org/10.1021/acsomega.1c01751
ACS Omega 2021, 6, 18737−18744

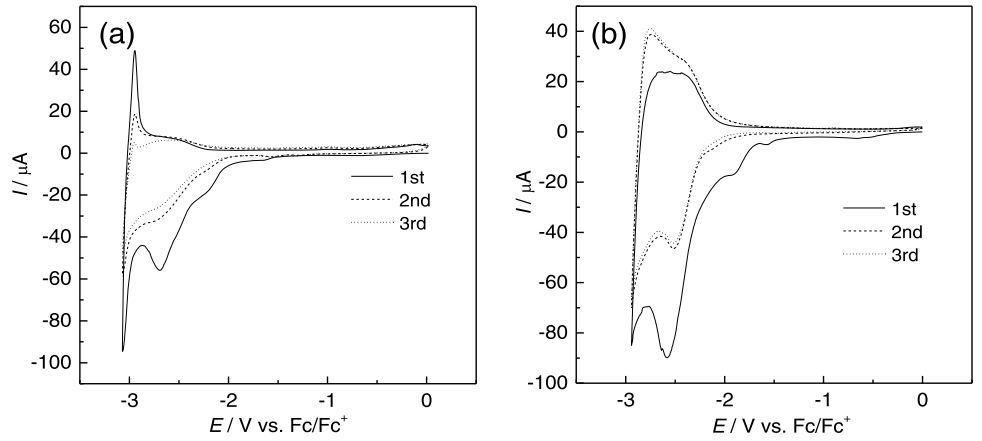

Figure 8. Cyclic voltammograms of CNS-1100 composite electrodes in (a) 0.9 and (b) 4 mol kg^{-1} NaTFSA/EC + DMC (1:1 by vol) at a scan rate of 0.1 mV s^{-1}.

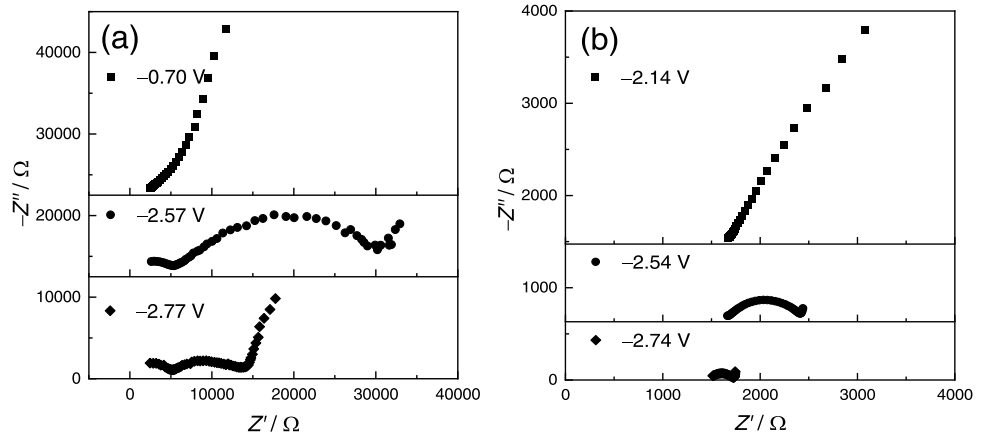

Figure 9. Nyquist plots of CNS-1100 composite electrodes in (a) 0.9 and (b) 4 mol kg^{-1} NaTFSA/EC + DMC (1:1 by vol).

calculating the heats of solvating reaction, and the rate-determining step was considered to be the final desolvation process.[12] Based on the previous reports,[25] solvents seem to be difficult to cointercalate into the bulk of low-crystallized carbons and desolvation process should be necessary for lithium-ion insertion into CNS-1100. Hence, the rate-determining step in the lithium-ion transfer reaction between the CNS electrode and the dilute electrolyte seemed to be the final desolvation process of EC. The activation energy in 4 mol kg^{-1} LiTFSA/EC + DMC (1:1 by vol) was 75 kJ mol^{-1} and very large. We speculated that the kinetics of the interfacial lithium-ion transfer reaction in concentrated electrolytes is controlled by the interaction between the lithium ion and anion, which might be stronger than the interaction between lithium ions and neutral solvents. These results were consistent with the previous reports of graphitized CNS.[17]

2.3. Sodium-Ion Transfer Reaction at the Interface between CNS Composite Electrodes/Organic Electrolyte Solutions. Figure 8 shows the CVs of CNS-1100 composite electrodes in 0.9 and 4 mol kg^{-1} NaTFSA/EC + DMC (1:1 by vol). The irreversible currents were observed in all of the electrolytes, and most of the irreversible currents disappeared from the 2nd cycle, indicating the formation of SEI on CNS electrodes in the same manner of the lithium-ion system. The redox peaks also appeared in all of the electrolytes and were assigned to the reversible sodium-ion insertion into/from CNS-1100. However, redox peaks in the dilute EC-based electrolyte decreased during cycling. This seemed to be because the SEI in the SIB system is easier to dissolve into electrolytes than that in the LIB system.[26] CNS has a large surface area owing to the small particle size, and the dissolution of SEI and degradation due to continuous electrolyte decomposition might be much severe. On the other hand, the redox peaks in concentrated electrolytes did not decrease during cycling, suggesting that the stability of SEI in concentrated electrolytes is the best. These results might be because the dissolution of SEI and the continuous electrolyte decomposition were the most minimized by the saturation of the high-salt-concentration electrolyte.

Figure 9 shows the Nyquist plots of the CNS-1100 composite electrode in 0.9 and 4 mol kg^{-1} NaTFSA/EC + DMC (1:1 by vol). At least one semicircle was observed at the middle-frequency region in all of the electrolytes. This semicircle at the middle-frequency region was assigned to the parallel circuits of charge-transfer resistances and capacitances like the cases of previous literatures.[17,27] The SEI resistance seemed to be negligible in the concentrated electrolytes because the amounts of SEI formation might also be minimized due to the best stability of SEI. In addition, only the interfacial sodium-ion transfer resistances in concentrated electrolytes were as small as the interfacial lithium-ion transfer resistances. The origin of the small interfacial resistance in the concentrated electrolyte might be derived from the high stability of SEI to prevent degradation of electrodes and large activity of sodium ion in concentrated electrolytes, which leads to large prefrequency factors. These

https://doi.org/10.1021/acsomega.1c01751
ACS Omega 2021, 6, 18737−18744

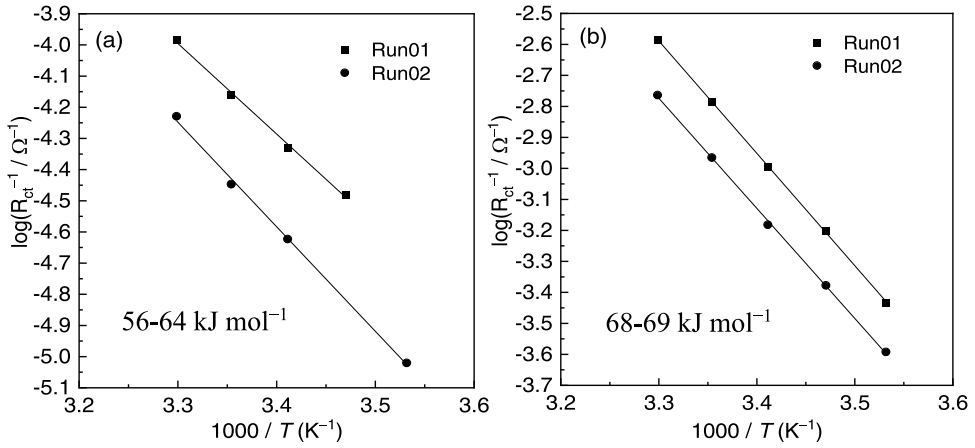

Figure 10. Temperature dependence of charge-transfer resistances of CNS-1100 composite electrodes in (a) 0.9 and (b) 4 mol kg^{-1} NaTFSA/EC + DMC (1:1 by vol).

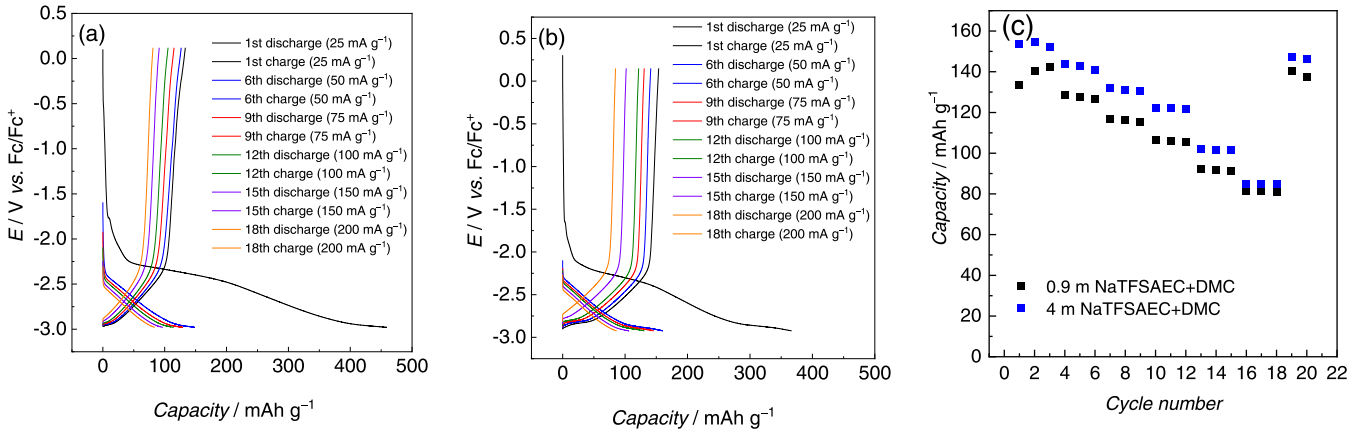

Figure 11. Charge−discharge curves of CNS-1100 and AB composite electrodes in (a) 0.9 and (b) 4 mol kg^{-1} NaTFSA/EC + DMC (1:1 by vol), and (c) reversible capacities plotted against the cycle number in both electrolytes.

results indicated that CNS-1100 negative electrodes in concentrated electrolytes can be the candidate of negative electrodes with high rate capability in SIBs.

The activation energies of the interfacial sodium-ion transfer at the interface between amorphous CNS and electrolyte solutions were evaluated in the same manner as that of the lithium system. Figure 10 shows the temperature dependence of charge-transfer reactions of CNS-1100 composite electrodes in 0.9 and 4 mol kg^{-1} NaTFSA/EC + DMC (1:1 by vol). The activation energy in 0.9 mol kg^{-1} NaTFSA/EC + DMC (1:1 by vol) was 56−64 kJ mol^{-1}. On the other hand, the activation energy in 4 mol kg^{-1} NaTFSA/EC + DMC (1:1 by vol) was 68−69 kJ mol^{-1} and very large. These values of activation energies were close to those of graphitized CNS electrodes.[17] Hence, the electrolyte dependency of activation energies of interfacial sodium-ion transfer seemed to be universal for carbonaceous electrodes independent of the graphitization degree. The activation energies of the interfacial sodium-ion transfer might be dependent on the interaction between sodium ions and solvents or anions. However, the rate-determining step of the interfacial sodium-ion transfer might not be the simple desolvation process but the multiple process because these values of activation energies of interfacial sodium-ion transfer were much larger than the expected values of activation energies decided by the simple desolvation process based on the weak Lewis acidity of sodium ion. Considering the large activation energies of sodium-ion transfer resistances in concentrated electrolytes, decreasing the activation energies is desired in the future to decrease the interfacial resistances due to changing the salt anions and so forth.

Finally, Figure 11 shows the charge−discharge curves of CNS-1100 and acetylene black (AB) composite electrodes in 0.9 and 4 mol kg^{-1} NaTFSA/EC + DMC (1:1 by vol). At the first cycle, the irreversible capacity of the CNS electrode in the dilute electrolyte was larger than that in the concentrated electrolyte, indicating that the passivation ability of SEI in the concentrated electrolyte was better than in the dilute electrolyte like the case of the cyclic voltammograms. The maximum reversible capacity of CNS-1100 electrodes was around 145 mAh g^{-1}. To evaluate the rate capability of CNS-1100 electrodes in both electrolytes, the reversible capacities were plotted against the cycling number, as shown in Figure 11c. Based on the result in Figure 11c, the rate capability of CNS-1100 electrodes in the concentrated electrolyte under medium current densities was better than in the dilute electrolyte. These results also indicated that internal resistances of CNS-1100 electrodes in the concentrated electrolyte can be smaller than in the dilute electrolyte. Under the largest current densities, capacity loss in the concentrated electrolyte was almost the same as in the dilute electrolyte. This seemed to be because IR drops in the concentrated electrolyte were larger than in the dilute electrolyte due to the smaller electrolyte conductivity and so on. Hence, decreasing the

https://doi.org/10.1021/acsomega.1c01751
ACS Omega 2021, 6, 18737−18744

activation energies of charge-transfer resistances and increasing electrolyte conductivities in concentrated electrolyte systems are desired to fabricate the high-rate sodium-ion battery in the future.

3. CONCLUSIONS

The interfacial sodium-ion transfer reaction at the interface between the CNS-1100 electrode and electrolyte solutions was investigated with comparison to the lithium-ion transfer reaction. From the cyclic voltammograms, both lithium ion and sodium ion can reversibly insert into/from CNS-1100 in all of the electrolytes. In the Nyquist plots, the semicircles at the high-frequency region and the middle-frequency region were assigned to the SEI resistance and the charge-transfer resistance, respectively. The activation energies of both interfacial lithium-ion and sodium-ion transfer resistances were also measured. The values of activation energies of both interfacial lithium-ion and sodium-ion transfer resistances were dependent on the composition of electrolytes. In addition, these values of the activation energies for amorphous CNS electrodes were close to those for graphitized CNS electrodes, suggesting that the activation energies of the interfacial sodium-ion transfer might be independent of the graphitization degree. The charge−discharge curves indicated the better rate capability of CNS-1100 and AB electrodes in sodium salt-concentrated electrolytes than in dilute electrolytes. To fabricate the SIBs with high rate capability, applying nanocarbonaceous negative electrodes with concentrated organic electrolyte solutions is one of effective approaches.

4. EXPERIMENTAL SECTION

Electrochemical measurements were carried out using a three-electrode cell. A CNS-1100 composite electrode (CNS-1100 (700−800 nm,[16,17] Tokai Carbon Co., Ltd.)/poly(vinylidene difluoride) (PVdF) = 80:20 wt %) was used as a working electrode. CNS-1100 electrodes used in cyclic voltammetry and electrochemical impedance spectroscopy did not contain conductive carbons to exclude the interfacial reaction of conductive carbons. For charge−discharge measurements, the CNS-1100 and AB composite electrodes (CNS-1100/AB (Denka)/PVdF = 78:2:20 wt %) were used. The Ag/Ag^+ electrode (silver wire immersed into EC + DMC (1:1 by vol) (Kishida Chemical Co., Ltd.) mixture containing 0.2 mol kg^{-1} of NaTFSA (Kishida Chemical Co., Ltd.) and 0.04 mol kg^{-1} of silver trifluoromethanesulfonate (Sigma-Aldrich)) was used as a reference electrode, and a natural graphite composite electrode (natural graphite/PVdF = 90:10 wt %) was used as a counter electrode. Electrolyte solutions were EC + DMC (1:1 by vol) (Kishida Chemical Co., Ltd.) mixture containing 0.9 and 4 mol kg^{-1} LiTFSA (Kishida Chemical Co., Ltd.) or NaTFSA. In this study, TFSA salts with high solubility were used to avoid the evolution of HF. The potential of the silver reference electrode was calibrated by measuring the redox potential of ferrocene in each electrolyte containing 3 mmol kg^{-1} of ferrocene (Alfa Aesar). Hereafter, all potentials are referred to as Fc/Fc^+; −2.77 and −2.74 V vs Fc/Fc^+ in 0.9 and 4 mol kg^{-1} NaTFSA/EC + DMC, respectively, were near to 0.2 V vs Na/Na^+. Cyclic voltammetry (CV) was conducted between open-circuit potential (OCV) and various potentials, and the scan rate was set at 0.1 mV s^{-1}. Electrochemical impedance spectroscopy was carried out with an ac amplitude of 10 mV in a frequency range of 100 kHz to 10 mHz at temperatures ranging from 30 to 10 °C. Charge−discharge measurements were conducted between OCV and −2.98 or −2.925 V vs Fc/Fc^+ in 0.9 or 4 mol kg^{-1} NaTFSA/EC + DMC, respectively, and the current densities were set between 25 and 200 mA g^{-1}. The cells were assembled in an Ar-filled glovebox. All electrochemical measurements were carried out using HSV-100 (HOKUTO-DENKO) and Solartron1470E+1400A (Solartron Analytical). SEM, XRD measurements, and Raman spectroscopy were used for structural characterization of CNS-1100 electrodes and electrolyte solutions using S-3000H (Hitachi High-Tech Fielding Corp.), RINT2200 (RIGAKU), and LabRAM HR (HORIBA).

AUTHOR INFORMATION

Corresponding Author

Yasuyuki Kondo − *Graduate School of Engineering, Kyoto University, 615-8510 Kyoto, Japan;* orcid.org/0000-0003-1103-3329; Email: yasuyuki.kondo@elech.kuic.kyoto-u.ac.jp

Authors

Tomokazu Fukutsuka − *Graduate School of Engineering, Nagoya University, 464-8603 Nagoya, Japan*

Yuko Yokoyama − *Office of Society-Academia Collaboration for Innovation, Kyoto University, 615-8510 Kyoto, Japan*

Yuto Miyahara − *Graduate School of Engineering, Kyoto University, 615-8510 Kyoto, Japan;* orcid.org/0000-0003-4662-0996

Kohei Miyazaki − *Graduate School of Engineering, Kyoto University, 615-8510 Kyoto, Japan; Element Strategy Initiative for Catalysts & Batteries, Kyoto University, 615-8246 Kyoto, Japan;* orcid.org/0000-0001-5177-3570

Takeshi Abe − *Graduate School of Engineering, Kyoto University, 615-8510 Kyoto, Japan; Element Strategy Initiative for Catalysts & Batteries, Kyoto University, 615-8246 Kyoto, Japan*

Complete contact information is available at: https://pubs.acs.org/10.1021/acsomega.1c01751

Notes

The authors declare no competing financial interest.

ACKNOWLEDGMENTS

This work was partially supported by the Element Strategy Initiative for Catalysts & Batteries (ESICB), Kyoto University.

REFERENCES

(1) Doughty, D.; Butler, P. C.; Skhil, A. A.; Clark, N. H.; Boyes, J. D. Batteries for large-scale stationary electrical energy storage. *Electrochem. Soc. Interface* **2010**, *19*, 49−53.

(2) Lu, L.; Han, X.; Li, J.; Hua, J.; Ouyand, M. A review on the key issues for lithium-ion battery management in electric vehicles. *J. Power Sources* **2013**, *226*, 272−282.

(3) An, Y.; Fei, H.; Zeng, G.; Ci, L.; Xiong, S.; Feng, J.; Qian, Y. Green, scalable, and controllable fabrication of nanoporous silicon from commercial alloy precursors for high-energy lithium-ion batteries. *ACS Nano* **2018**, *12*, 4993−5002.

(4) Zeng, G.; An, Y.; Xiong, S.; Feng, J. Nonflammable fluorinated carbonate electrolyte with high salt-to-solvent ratios enables stable silicon-based anode for next-generation lithium-ion batteries. *ACS Appl. Mater. Interfaces* **2019**, *11*, 23229−23235.

(5) Yabuuchi, N.; Kubota, K.; Dahbi, M.; Komaba, S. Research development on sodium-ion batteries. *Chem. Rev.* **2014**, *114*, 11636−11682.

(6) Dahbi, M.; Yabuuchi, N.; Kubota, K.; Tokiwa, K.; Komaba, S. Negative electrodes for Na-ion batteries. *Phys. Chem. Chem. Phys.* **2014**, *16*, 15007−15028.
(7) Komaba, S.; Murata, W.; Ishikawa, T.; Yabuuchi, N.; Ozeki, T.; Nakayama, T.; Ogata, A.; Gotoh, K.; Fujiwara, K. Electrochemical Na insertion and solid electrolyte interphase for hard-carbon electrodes and application to Na-ion batteries. *Adv. Funct. Mater.* **2011**, *21*, 3859−3867.
(8) Yoshizawa, N.; Tanaike, O.; Hatori, H.; Yoshikawa, K.; Kondo, A.; Abe, T. TEM and electron tomography studies of carbon nanospheres for lithium secondary batteries. *Carbon* **2006**, *44*, 2558−2564.
(9) Maruyama, S.; Fukutsuka, T.; Miyazaki, K.; Abe, Y.; Yoshizawa, N.; Abe, T. Lithium-ion intercalation and deintercalation behavior of graphitized carbon nanospheres. *J. Mater. Chem. A* **2018**, *6*, 1128−1137.
(10) Ogihara, N.; Kawauchi, S.; Okuda, C.; Itou, Y.; Takeuchi, Y.; Ukyo, Y. Theoretical and experimental analysis of porous electrodes for lithium-ion batteries by electrochemical impedance spectroscopy using a symmetric cell. *J. Electrochem. Soc.* **2012**, *159*, A1034−A1039.
(11) Amemiya, T.; Fujishima, A. Electrochemical impedance spectroscopy. Variety of transfer function analysis. *Denki Kagaku* **1993**, *61*, 290−294.
(12) Fukutsuka, T.; Sagane, F.; Miyazaki, K.; Abe, T.; Toda, T.; Matsuo, Y.; Sugie, Y.; Ogumi, Z. Ion-solvent interaction for lithium-ion transfer at the interface between carbonaceous thin-film electrode and electrolyte. *TANSO* **2010**, *2010*, 188−191.
(13) Ishihara, Y.; Miyazaki, K.; Fukutsuka, T.; Abe, T. Lithium-ion transfer at the interface between high potential negative electrodes and ionic liquids. *J. Electrochem. Soc.* **2014**, *161*, A1939−A1942.
(14) Yamada, Y.; Iriyama, Y.; Abe, T.; Ogumi, Z. Kinetics of lithium ion transfer at the interface between graphite and liquid electrolytes: effects of solvent and surface film. *Langmuir* **2009**, *25*, 12766−12770.
(15) Abe, T.; Sagane, F.; Ohtsuka, F.; Iriyama, Y.; Ogumi, Z. Lithium-ion transfer at the interface between lithium-ion conductive ceramic electrolyte and liquid electrolyte-a key to enhancing the rate capability of lithium-ion batteries. *J. Electrochem. Soc.* **2005**, *152*, A2151−A2154.
(16) Sagane, F.; Abe, T.; Ogumi, Z. Sodium-ion transfer at the interface between ceramic and organic electrolytes. *J. Power Sources* **2010**, *195*, 7466−7470.
(17) Kondo, Y.; Fukutsuka, T.; Yokoyama, Y.; Miyahara, Y.; Miyazaki, K.; Abe, T. Kinetic properties of sodium-ion transfer at the interface between graphitic materials and organic electrolyte solutions. *J. Appl. Electrochem.* **2021**, *51*, 629−638.
(18) Takada, K.; Yamada, Y.; Watanabe, E.; Wang, J.; Sodeyama, K.; Tateyama, Y.; Hirata, K.; Kawase, T.; Yamada, A. Unusual passivation ability of superconcentrated electrolytes toward hard carbon negative electrodes in sodium-ion batteries. *ACS Appl. Mater. Interfaces* **2017**, *9*, 33802−33809.
(19) Kondo, Y.; Fukutsuka, T.; Miyahara, Y.; Miyazaki, K.; Abe, T. Sodium-ion intercalation behavior of graphitized carbon nanospheres covered with basal plane. *Chem. Lett.* **2019**, *48*, 799−801.
(20) Song, H.-Y.; Fukutsuka, T.; Miyazaki, K.; Abe, T. In situ Raman investigation of electrolyte solutions in the vicinity of graphite negative electrodes. *Phys. Chem. Chem. Phys.* **2016**, *18*, 27486−27492.
(21) Castriota, M.; Caruso, T.; Agostino, R. G.; Cazzanelli, E.; Henderson, W. A.; Passerini, S. Raman investigation of the ionic liquid N-methyl-N-propylpyrrolidinium bis(trifluoromethanesulfonyl)imide and its mixture with $LiN(SO_2CF_3)_2$. *J. Phys. Chem. A* **2005**, *109*, 92−96.
(22) Jeong, S.-K.; Inaba, M.; Iriyama, Y.; Abe, T.; Ogumi, Z. Interfacial reactions between graphite electrodes and propylene carbonate-based solutions: Electrolyte-concentration dependence of electrochemical lithium intercalation reaction. *J. Power Sources* **2008**, *175*, 540−546.
(23) Abe, T.; Fukuda, H.; Iriyama, Y.; Ogumi, Z. Solvated Li-ion transfer at interface between graphite and electrolyte. *J. Electrochem. Soc.* **2004**, *151*, A1120−A1123.
(24) Doi, T.; Iriyama, Y.; Abe, T.; Ogumi, Z. Lithium-ion transfer at an electrolyte/heat-treated nongraphitizable carbon electrode interface. *J. Electrochem. Soc.* **2005**, *152*, A1521−A1525.
(25) Inagaki, M.; Tanaike, O. Determining factors for the intercalation into carbon materials from organic solutions. *Carbon* **2001**, *39*, 1083−1090.
(26) Mogensen, R.; Brandell, D.; Younesi, R. Solubility of the solid electrolyte interphase (SEI) in sodium ion batteries. *ACS Energy Lett.* **2016**, *1*, 1173−1178.
(27) Hasegawa, G.; Kanamori, K.; Kannari, N.; Ozaki, J.; Nakanishi, K.; Abe, T. Studies on electrochemical sodium storage into hard carbons with binder-free monolithic electrodes. *J. Power Sources* **2016**, *318*, 41−48.

https://doi.org/10.1021/acsomega.1c01751
ACS Omega 2021, 6, 18737−18744